

## IMECE2003-41446

### BIOMIMETIC COMPLIANT SYSTEM FOR SMART ACTUATOR-DRIVEN AQUATIC PROPULSION: PRELIMINARY RESULTS

**Brian P. Trease**

Dept. of Mechanical Engineering  
The University of Michigan  
Ann Arbor, MI 48109  
trease@asme.org

**Kerr-Jia Lu**

Dept. of Mechanical Engineering  
The University of Michigan  
Ann Arbor, MI 48109  
kjl@umich.edu

**Prof. Sridhar Kota**

Dept. of Mechanical Engineering  
The University of Michigan  
Ann Arbor, MI 48109  
kota@umich.edu

#### ABSTRACT

Biomimetic design takes principles from nature to employ in engineering problems. Such designs are hoped to be quiet, efficient, robust, and versatile, having taken advantage of optimization via natural selection. However, the emulation of specific biological devices poses a great challenge because of complicated, arbitrary, and over-redundant designs. Compliant mechanisms are of immediate appeal in addressing the problem of complex, biomimetic deformation because of their inherent flexibility and distributed compliance. The goal of this research is to develop a biologically-inspired hydrofoil for aquatic propulsion, by assembling planar compliant mechanism building blocks to generate complex 3-D deformations. The building block is a rib structure generated from topology optimization. An ADAMS model is then created to quickly visualize motion and estimate system characteristics. System refinement is achieved through further size and shape optimization of individual ribs. Testing of a single-rib and dual-actuator system is currently in progress. The preliminary results have demonstrated the potential of this combined approach to quickly identify and evaluate new applications that may result from building blocks.

*KEYWORDS: compliant mechanism synthesis, biomimetic fin, aquatic propulsion, active hydrofoil, spatial deformation*

#### 1. INTRODUCTION

##### 1.1. Biomimetic Aquatic Design

Biologically-inspired design, or biomimetics, is both the inspiration and result of research in a number of new areas including compliant mechanisms, smart materials, biorobots, neural-based controls, and design for auto-assembly (or no-assembly). Biomimetic design takes principles from nature to employ in engineering problems. Examples cover a broad range of categories, including Velcro, fibrous composites,

hexapedal robots, and the self-cleaning Lotus-Effect® [1]. The example driving our current investigation is the emulation of biological aquatic propulsion. Such projects include a shape-memory-alloy actuated biomimetic hydrofoil [2, 3], an active polymer driven underwater micro robot [4], and the conventionally actuated RoboTuna [5] and Robot Pike [6]. These technologies seek to provide a means for quiet and efficient propulsion with an increased degree of maneuverability. Potential applications include general aquatic locomotion research, military reconnaissance and decoys, search and rescue devices, video exploration, and remote maintenance operations.

Many of the previous design efforts are based on two-dimensional mechanisms, but a variety of aquatic propulsion observed in nature requires complex 3-D deformations. Efficient maneuvering demands even more deformation capabilities. Thus far, this complexity has been difficult to achieve, partly because elasticity has not yet been taken advantage of to the degree as it is used in nature's designs.

##### 1.2. Compliant Mechanisms

Compliant mechanisms are of immediate appeal in addressing the problem of complex, biomimetic deformation. Also biologically inspired in principle, compliant mechanisms take advantage of flexure to achieve transmission of motion and force, rather than the rigid-body mechanisms used in traditional engineering design. The synthesis of these mechanisms has been well studied, and their advantages have been well documented [7-10], including: absence of wear, backlash, and friction and ease of manufacture. Furthermore, the smooth and continuous deformations of compliant mechanisms are particularly suited to the fluid dynamics of aquatic applications, as opposed to the discrete links and joint/seam discontinuities in rigid-link devices. A fully-compliant system also has great stealth potential for both aquatic and aeronautical craft.

Smooth, continuous deformations result in a much less distinguished sonar “signature”, but even if spotted, biomimetic vessels may be mistaken for their biological precedents.

Observing nature is often a source of inspiration for compliant mechanism design, but none have yet attempted to emulate specific biological devices. The complicated, arbitrary, and over-redundant designs of nature pose a greater challenge than previously-developed compliant mechanisms, most of which are single-input, single-output, planar designs. How can we develop more complex, multi-degree-of-freedom, 3-D systems? This research explores an extension of 2-D devices to achieve 3-D deformation. Lu and Kota [11, 12] have reported compliant mechanisms designed for shape change in two-dimensions. In specific applications with 3-D structures (e.g. an airfoil), the design domain is sliced into 2-D regions and planar mechanism synthesis proceeds. While this shape control is a starting point for achieving specific deformations, we are now looking beyond planar and parallel sections and at the potential of using non-parallel mechanisms. Another important aspect of this research is the concept of “building-blocks” to create compliant biomimetic systems from similar compliant components.

This paper looks at the design of a compliant mechanical system for an active, propulsion-generating hydrofoil, which may eventually be incorporated into a fully-compliant mechanical fish. With only preliminary design results and physical testing still in progress, the most important contribution of this paper is our design methodology. This paper illustrates the overall procedure, from building block, to system, to optimization of the components. The problem definition given below is specifically for pectoral fin locomotion, but our procedure is also applicable to other system designs, such as the undulatory eel fin described later in Section 4. Motion analysis software with flexible element capability (i.e. ADAMS) allows us to quickly evaluate several aspects of new systems: rapid trials of various spatial arrangements of the compliant components, calculation of the volume swept by the resulting compliant hydrofoil, and evaluation of stroke path with both quantitative data and instant visualization for assessment of feasibility.

## 2. GENERAL PROBLEM DEFINITION

The fin waveform of the *bird wrasse* fish (Fig. 1) was chosen as the target motion in the development of a mechanical hydrofoil system. The wrasse fish creates 10mN of force at a stroke frequency of 2.9 to 4.2 Hz, attaining speeds from 22 cm/s to 50 cm/s, with a 21cm overall body length [13]. Specifically, we are focusing on the oscillatory (stroke) motion of the pectoral (lateral) fins, which provide most of the propulsion for the wrasse. The waveform is defined by a set of biological data points that trace markers on the trailing edge of the wrasse fin over one stroke cycle [13]. Complex motion generation is achieved by using various-length building blocks in parallel, similar to the bone structure found in the biological fins. The series of adjacent compliant ribs emanate outward from the aquatic vessel’s main body. Completing the fin will

be an elastic skin over and connecting the outside edges of adjacent ribs.

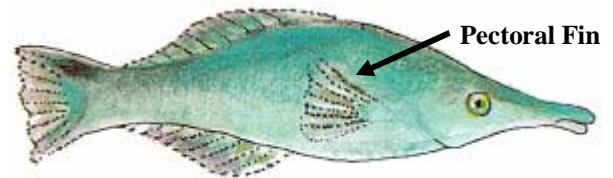


**Figure 1: Bird Wrasse (*Gomphosus caeruleus*)**  
Image Copyright © 1996-2003 by Paolo Vecchi

To create a compliant hydrofoil system from compliant components, a building block approach is used. The essential element of the system is chosen to be a compliant rib. A compliant rib is an active, flexible skeletal structure, controlled by two linear actuators to create tip motion and rib curvature. Section 3 focuses on the topology (form) of the individual ribs, which is then used in Section 4 to look at the feasibility of the system as a whole. Finally, in Section 5, the ribs are optimized to match the requirements of the entire system.

## 3. FIN TOPOLOGY GENERATION

### 3.1. Symmetric Design Domain

The goal of topology synthesis is to create a fin rib topology that can generate a symmetric, bidirectional stroke motion, similar in appearance to that of a fish tailfin. While neither observed nor required in pectoral fins, symmetry significantly simplifies the bidirectional stroke design problem.

As shown in Fig. 2, two linear actuators actuate the fin rib antagonistically. When one actuator is activated, the other is assumed to be fixed in its original position, causing the whole structure to bend toward the actuated side. Alternating the order of actuation generates an alternating waveform, from Motion I to Motion II. The design domain is defined by the dashed lines depicting the fin outline. The compliant rib structure should fit within the triangular design domain, to maintain a smooth external surface. The rib structure must also be symmetric about the x-axis in order to facilitate symmetric stroke motion.

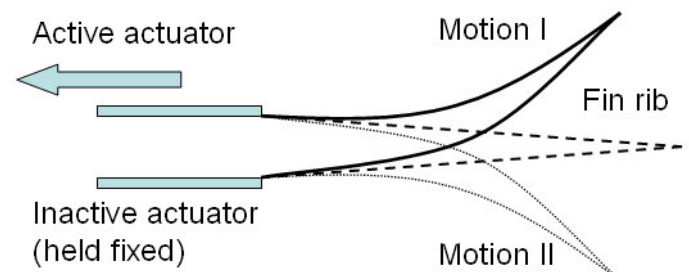


**Figure 2: Fin Rib with Bi-directional Stroke Motion**

In addition, two sets of loading and support boundary conditions (Fig. 3) are investigated in the topology synthesis: (BC1) the actuators are attached directly to the rib structure boundary; and (BC2) the actuators are located within the rib boundary. The two actuator locations are also symmetric about the x-axis, to maintain subsequent symmetry of the structure. Again, the desired structure can operate in either direction,

depending of which actuator is currently active. Consequently, when one actuator is active, the other inactive actuator is required to bear a compressive load equal to the force output of the active actuator.

While establishing our symmetric design space for the goal of bidirectional output, we have not fixed any part of the rib directly to a ground. Rather, all ground connections are via either actuators or sliding joints.

### 3.2. Naval Research Laboratory Collaboration

For the topology synthesis, the initial design parameters are based on our collaboration with the Naval Research Laboratory (NRL) to demonstrate the performance of a *single* compliant rib. The specified design domain is 100mm in total rib length and 10mm across at the base of the rib. The ribs are being designed for integration with the NRL's high-force liquid-crystal elastomer actuators. These compact linear actuators (4mm by 4mm cross-sections) are capable of forces from 1N to 4N and 20% actuation strain [14]. Our formulation assumes the actuators provide 1N of contraction force with a maximum input displacement of 5mm. The material used for the fin rib is ABS plastic, chosen for its use in our Rapid Prototyping machine (Young's Modulus: 2480MPa, Yielding Stress: 34.45MPa). The desired deflection for the fin rib is at least 15% of the total rib length, i.e. 15mm.

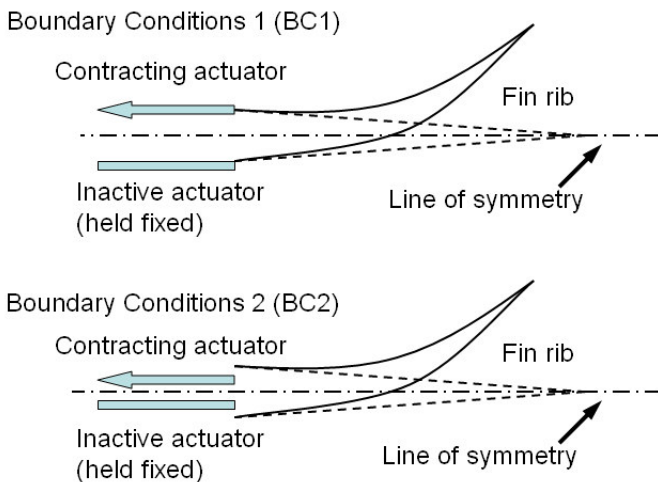


Figure 3: Alternate Sets of Boundary Conditions

### 3.3. Topology Synthesis Methods

Various systematic compliant mechanism synthesis approaches [11, 12], using structural optimization techniques, have been developed in the past decade to optimize the material distribution (topology) within a specified design domain. The synthesis approach generally requires a design domain parameterization to represent various topologies in terms of the design variables. An optimization procedure is then used to find the optimal values of the design variables. Employ Continuous and discrete optimization techniques have been adopted depending on the types of the design variable.

In this research, two approaches are employed to synthesize the fin rib structure, based on the selection of an appropriate objective function. One possible objective is simply to create motion at the tip of the rib. When the tip is considered an output port and the actuator an input port, the objective function is to maximize the geometric advantage (output displacement/input displacement) under a specified force input. This objective function is incorporated into a grounded-structure approach using a continuous optimization method. Fin stroke deformation can also be seen as a shape-change problem with multiple outputs. Thus, shape-matching is another possible goal, using least square error of deviation from points on a target curve as the objective function. This objective function is optimized with the load-path representation approach combined with a Genetic Algorithm (GA). The load-path approach was originally designed to accommodate such shape-morphing problems. The details of both optimization approaches are included in the Appendix.

### 3.4. Results

The combinations of different optimization methods and objective functions result in several different topologies, seen in Figs. 4 and 5. The results of the grounded-structure methods are used for (BC1), while the results of the load-path method are used for (BC2). See the appendix for the explanation of these choices.



Figure 4: Result for BC1

Figure 5: Result for BC2

Before going into further size and shape optimization of the newly generated device topologies, it is beneficial to focus on one design and how it extrapolates to form an entire system. Because of its simplicity, the rib topology for BC2 (Fig. 5) is chosen as a building block to construct several preliminary three-dimensional fin systems. Creating a model to visualize the operation of a whole fin system aids in understanding the required motion for each rib and how to operate the actuators. Such information is needed before proceeding to optimization of each rib.

## 4. BUILDING BLOCK APPROACH

Motion analysis in ADAMS provides rapid insight into how a system can be built up from multiple compliant ribs. These preliminary analyses demonstrate the ability of two-dimensional compliant components to create complex three-dimensional deformation. In addition to motion visualization, the preliminary studies offer actuator and force data to aid in further customization of all of the rib topologies.

While each rib provides the previously-described basic deflection, more complex warping and stretching motion is required to match the overall fin deformation and curvature observed over the stroke cycle [13]. Taking advantage of the parallel rib arrangement leads to several possibilities for more complex motion. The first method (Fig. 6) is accomplished by operating parallel ribs out-of-phase, resulting in 3-D warping of

the outer connecting skin. The other method is to use “angled ribs”, i.e. ribs deflecting in non-parallel planes (See Fig. 7). Thus, even during in-phase operation, the tips of two adjacent ribs will move toward and away from each other.

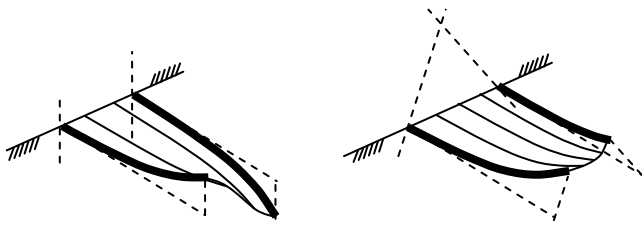


**Figure 6:** Out-of-phase ribs

**Figure 7:** Angled Ribs

Based on the above principles, three designs have been proposed as feasible hydrofoil systems (Figs. 8 – 10). These three designs are used to investigate system feasibility and provide motivation and system-level data for more detailed component design. System-level data includes stroke path and total fluid volume swept. Two of the designs (Pectoral-1 and Pectoral-2), exhibit oscillatory (stroke) motion. The third design (Undulating Fin) demonstrates another possible means of aquatic propulsion, akin to the undulatory fin motion seen in eels and rays.

All three designs use the method of out-of-phase rib deflections to achieve proper fin deformation, while Pectoral-1 further employs the method of angled ribs. The first two designs also incorporate additional rotary actuation to create larger bulk rotation of the hydrofoil. Pectoral-2 requires three such additional actuators, while Pectoral-1 requires only one. However, the angled ribs of Pectoral-1 help to compensate for its fewer degrees of freedom.

The undulatory motion of the Undulating Fin is a very different approach to propulsion. While the Undulating Fin is not designed to match any specific biological waveform data, it is believed to be an idealized demonstration of how compliant systems are easily and well fit for aquatic propulsion. It creates a sinusoidal undulating motion along a lateral fin to provide propulsion. When not providing propulsion, the many ribs can be deformed to achieve complex spatial configurations for maneuverability.

#### 4.1. System Visualization and Analysis

The designs were simulated in ADAMS for motion and force analysis of the entire system. The topologies used are those obtained from the previous topology generation step, and thus the size and shape of the beams are still considered to be variable. Nominal thickness values are therefore chosen for implementation in the system motion analysis. The range of motion and stress analyses for each rib (calculated with nonlinear finite element analysis), are therefore only estimates, but still relevant in evaluating the entire system at this stage. These estimates are applied as the limits of motion in the ADAMS models.

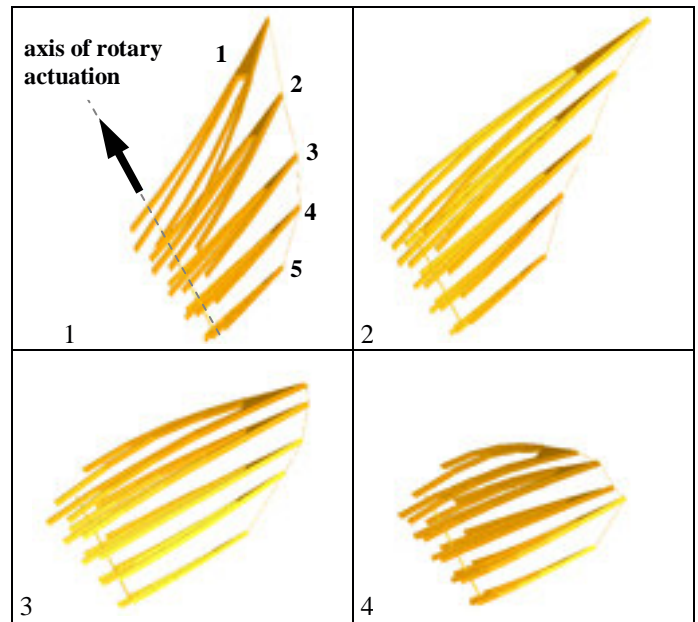


**Figure 8(1-4):** Pectoral-1 Fin Design

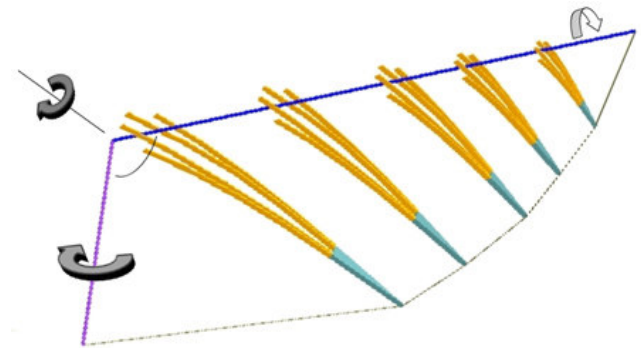


**Figure 9:** Pectoral-2 Fin Design  
(axes of the 3 rotary actuators are indicated)

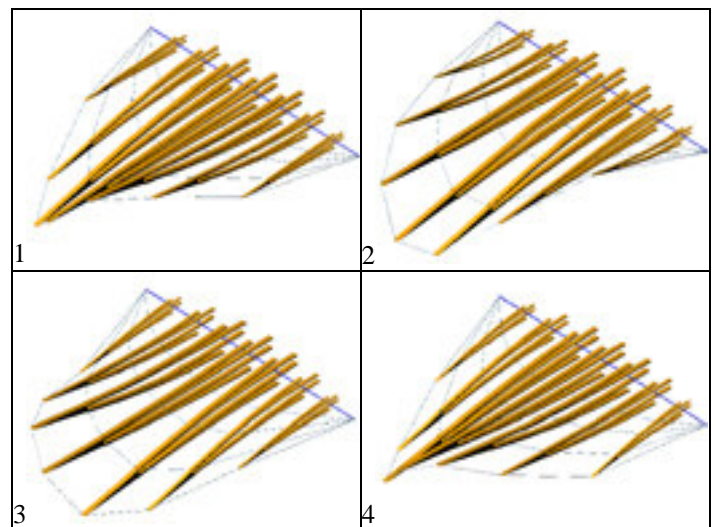


**Figure 10(1-4):** Undulating Fin Design

#### 4.2. Results

The most substantial result is the qualitative achievement of a fin stroke motion with proper deformation. This is portrayed in

Figs. 8 and 10 and more easily in video animations (See the digital appendix). The simulations indicate that Pectoral-2 most closely matches the stroke motion of the wrasse fish.

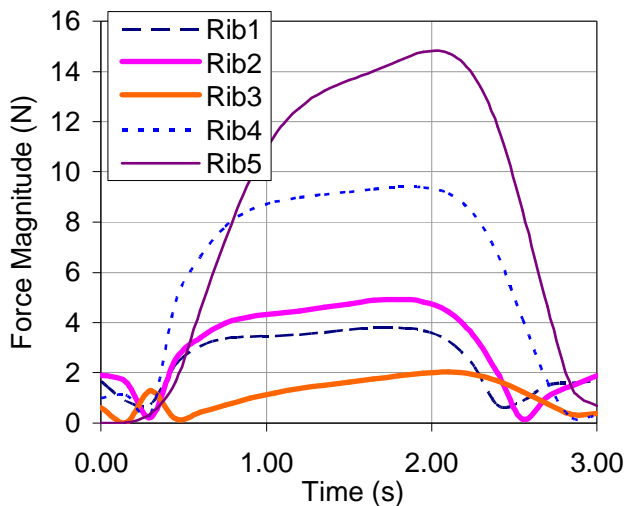
Another important system characteristic, related to efficiency, is complexity. Complexity is indicated by the number and type of actuators required, and is shown in Table 1. Although the use of more actuators yields more degrees-of-freedom in creating complex deformation, the complexity of manufacture and operation also increases.

**Table 1: System Complexity / Number of Actuators**

Design	Linear Actuators	Rotary Actuators	Total Actuators
Pectoral-1	10	1	11
Pectoral-2	10	3	13
Undulating Fin	14	0	14

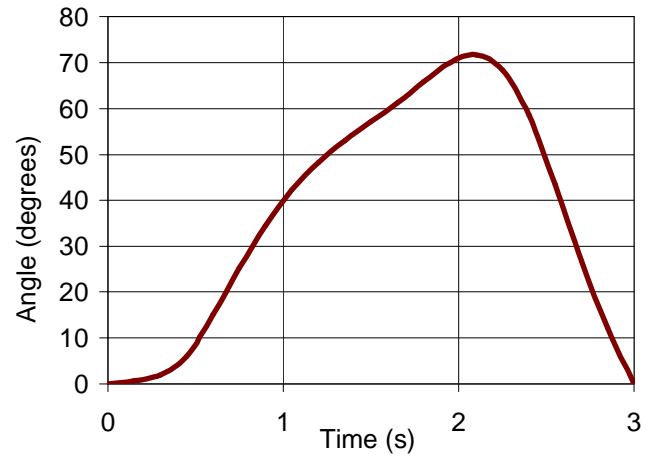
Single- and zero-rotary-actuator systems are simpler in form and take the most advantage of the compliant components. The optimal combination of compliance and actuation is yet to be determined, but the comparison of the models allows for investigation of this tradeoff. We see additional rotary actuators as an even greater increase in complexity and a digression from the goal of truly compliant systems. In addition, linear actuation is preferred because of the wide range of smart materials that can be used. Specific advantages of smart materials include compactness, lightness, and low noise levels.

Figure 11 depicts a time-history of required actuation forces over a 3-second stroke cycle (1/3 Hz). While the analysis is for operation in air (i.e. no hydro-dynamic forces are applied), it portrays an estimate of the required forces. The bulk rotation required of the rotary actuator is also shown in Fig. 12.



**Figure 11: Actuator Forces for Pectoral-1 Stroke Cycle**

Reviewing the actuator forces, most are higher than those capable of the NRL's actuators. This drives the need for refinement of the rib designs, which is done with size and geometry optimization in the next section.



**Figure 12: Rotation of Hinge for Pectoral-1 Stroke Cycle**

While the actuator forces describe system operation, a more relevant system characteristic is the propulsive force output. Analyses and experiments to determine the propulsive force are among the near future steps of this research.

## 5. SIZE AND GEOMETRY OPTIMIZATION

The size and geometry of two rib topologies are optimized to better match actuator performance and achieve specific system characteristics. This second optimization does not vary the topology, but only the thicknesses of the elements and the locations of the vertices. The resulting structure should be the stiffest possible structure that will achieve the desired deformation. Such a structure is more likely to resist hydrodynamic loads during propulsion. This is accomplished by minimizing the quantity:  $(total\ strain\ energy / geometric\ advantage)$ , to best satisfy the conflicting design requirements, rather than only maximizing *geometric advantage* as done in topology generation. Details of the size and geometry optimization are in the appendix and the results are shown below.

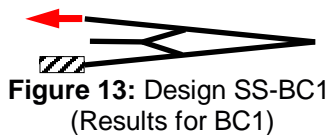


**Figure 13: Design SS-BC1 (Results for BC1)**

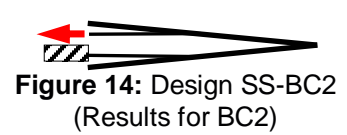


**Figure 14: Design SS-BC2 (Results for BC2)**

The maximum tip displacement for SS-BC1 and SS-BC2 are 15.0 and 14.9mm, respectively, meeting all design specifications. However, the structures have been designed for stiffness to resist external loads only by means of choosing to minimize the strain energy. Once the external hydrodynamic forces are known, verification of the stated deformations within all of the stress and actuator limits must be performed. If failure occurs under these loads, the optimization routines will be performed again, with the hydrodynamic forces included in the boundary conditions. Frequency analysis of the system must also be performed to ensure that operation occurs at or below the first natural frequency.

## 6. SINGLE COMPLIANT RIB DEMONSTRATION

This research describes only the first part of a larger project to create an autonomous aquatic vehicle propelled by our compliant fin system. Before assembling the entire system, we first look at fabricating and testing the individual building blocks, in collaboration with the NRL. The two rib topologies resulting from size and geometry optimization in the previous section were modified to provide custom 1N designs for the NRL, with deflections predicted by nonlinear FEA. Both ribs are 100mm by 10mm in overall dimensions, with 4mm out-of-plane thickness. The resulting designs (listed in Table 2) were fabricated in ABS plastic at the University of Michigan and tested at the NRL. One of the devices is shown in Fig. 15. Results are pending from the NRL, and will be included in the final version of this paper.

**Table 2:** Summary of rib designs for physical testing

Design:	NRL-BC1	NRL-BC2
Actuator Force Required (N)	1	1
Input Displacement (mm)	0.72	1.75
Output Displacement (mm)	14.9	16.0
Maximum Stress (MPa)*	9.4	8.3

\* Yield Stress for ABS Plastic is 34.45 MPa

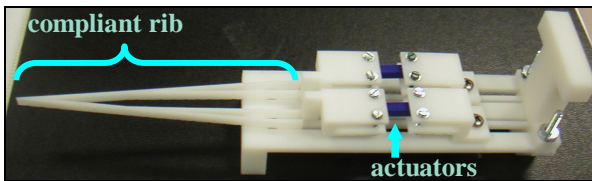


**Figure 15:** Rib Fabricated for Testing at the NRL  
Note: Design is for BC2

## 7. SUMMARY AND FUTURE WORK

In this paper, we have illustrated the design procedure to create a 3-D aquatic fin for propulsion from planar compliant building blocks. The combination of the ADAMS model with the structural optimization process allows us to quickly visualize and estimate the system performance. The preliminary results have demonstrated the potential of this whole approach to quickly identify and evaluate new applications that may result from building blocks.

Ongoing work involves refinement of the optimization models to include external hydrodynamic loads and frequency analysis for dynamic range of operation. Fluid volume swept during stroke can be calculated, along with the estimation of propulsive force generation, both experimentally and numerically. Fabrication of a complete hydrofoil prototype is required, beginning with several actuator/rib components operating in parallel.

## APPENDIX

### A1. TOPOLOGY GENERATION METHODS

#### A1.1. Grounded-Structure Approach

The grounded-structure approach first discretizes the design domain into a finite element mesh, and the structural topology is determined by the presence or elimination of each element.

A topology variable is assigned to each element to describe the element cross-section dimension. These design variables can continuously vary between a lower and an upper bound, where the lower bound is typically very close but not equal to zero, such as  $10^{-5}$ , to avoid the stiffness matrix singularity in the finite element analysis (FEA). The optimal cross-section dimensions are then determined using a continuous optimization method. When a topology variable converges to the lower bound, the element is considered eliminated from the mesh, hence obtaining the optimal topology.

Figure 16 shows parameterization of the design domain (not drawn to scale) for the rib structure with BC1. The initial discretization mesh is comprised of linear beam elements. It is assumed that the out-of-plane dimensions for all beams are held fixed, while the in-plane dimensions are allowed to vary between a lower and upper bound as design variables. In order to create a symmetric structure, the design domain is further reduced to the upper half of the triangular area. The complete topology is obtained by mirroring the upper design domain about the line of symmetry. That is, an element in the lower half design domain will share the same design variable with the corresponding element in the upper half. Note, however, that the boundary conditions are asymmetric, since one actuator is held fixed while the other one is activated. This initial discretization mesh is also used to incorporate BC2 by changing the actuator and support locations.

BC1

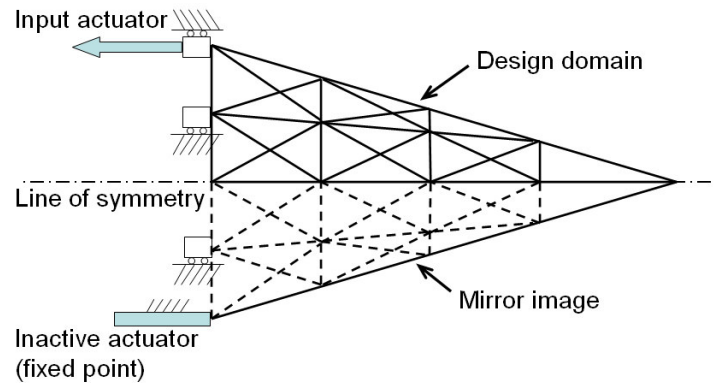


**Figure 16:** Design Domain for Grounded Structure

The overall dimensions of the design domain are 100mm by 10mm. Based upon the initial mesh shown in Fig. 16, the topology optimization problem formulation is shown in Eq. (1) ~ (6). The objective is to maximize the geometric advantage when actuated by a 1N linear actuator. Equation (2) is an equilibrium statement that represents the finite element method. The constraints include the lower and upper bounds for the design variables, the limit on maximum input displacement, and minimum tip displacement to ensure the desired rib motion can be achieved. All elements have a constant out-of-plane dimension of 4mm, and the in-plane beam dimensions ( $h_{\text{boundary}}$  and  $h_{\text{interior}}$ ) are optimized. The lower bound of the rib boundary dimension (i.e. elements on the external diagonal edge of the design domain) is set

significantly larger than that of the interior elements, because the rib boundary cannot be eliminated.

$$\text{maximize } Geometric\ Advantage \quad (1)$$

Subject to

$$d = K^{-1}F \quad (2)$$

$$0.5mm \leq h_{boundary} \leq 2mm \quad (3)$$

$$0.01mm \leq h_{interior} \leq 2mm \quad (4)$$

$$d_{input} < 5mm \quad (5)$$

$$d_{tip} > 15mm \quad (6)$$

The optimal topology, shown in Fig. 17, is obtained for BC1, using the sub-problem method in Ansys FEA software. The optimal topology for BC2 is coincidentally identical to that in Fig. 17.

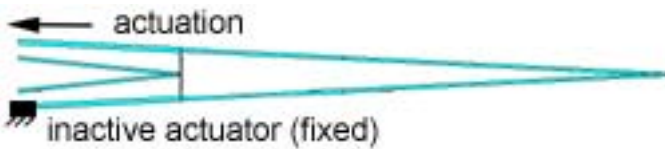


Figure 17: Design GS-BC1 (GS-BC2 is identical)

### A1.2. Load-path Approach

The load-path representation [12] is a design domain parameterization that represents the structural topology in terms of the physical connections between the input and the output points. These physical connections are the load-paths through which the energy from the input actuator can be delivered to output points. The structural topology is determined by the presence/absence of each path as well as the connectivity between different paths. A binary topology variable is assigned to each load-path to represent the presence of the path, while a set of intermediate connection ports controls the connectivity between different paths. This representation is incorporated into a genetic algorithm to synthesize shape morphing compliant mechanisms.

Figure 18 shows an example topology using the load-path representation with BC2. The design domain is again reduced to only the upper half of the triangular area in order to preserve symmetry. To incorporate the symmetry into the load-path representation, some fixed points are replaced by the symmetry points to generate paths between the design domain and the mirrored region. All paths in the design domain are mirrored about the line of symmetry to complete the structure. Five connection ports are used in this design to control the intermediate connections between different paths. The locations of the connection ports may also wander within the design domain to create various topologies. Interested readers can refer to Lu and Kota [12] for more details on the load-path representation.

Figure 19 shows how the topology changes according to the binary topology variables. The connection port locations are the same in Figs. 18 and 19, but the binary topology variables listed in Table 3 have different values (e.g. paths 1, 4, and 13). Furthermore, the locations of the intermediate connection ports (e.g. node 11) can also wander within the design domain, leading to yet another different topology, shown in Fig. 20.

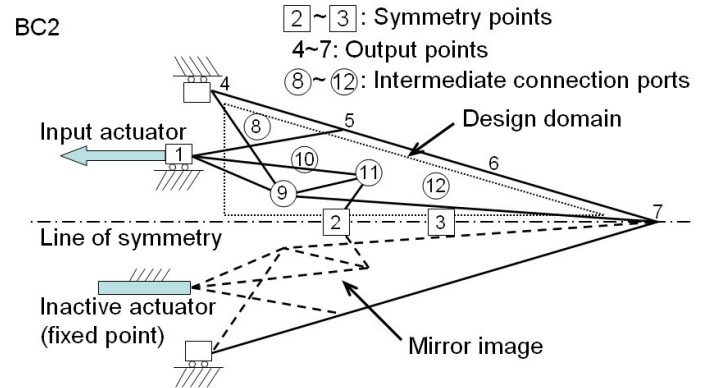


Figure 18: Example topology for Load-Path method

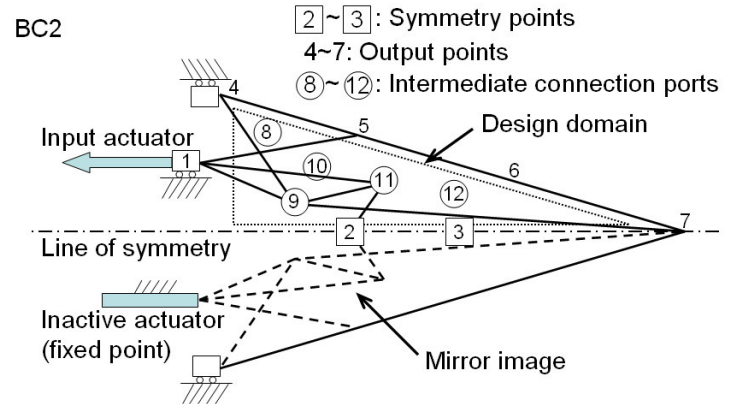


Figure 19: Effect of changing binary topology variables

Table 3: Topology Variables used in Figs. 18 and 19

Path type	Path No.	Path sequence	pTop <sub>i</sub> Fig. 18	pTop <sub>i</sub> Fig. 19
in ↓ out	1	{1,9,4}	1	0
	2	{1,5}	1	1
	3	{1,10,6}	0	0
	4	{1,11,9,7}	1	0
in ↓ sym	5	{1,11,2}	1	1
	6	{1,8,3}	0	0
sym ↓ out	7	{2,9,4}	0	0
	8	{2,5}	0	0
	9	{2,8,6}	0	0
	10	{2,7}	0	0
	11	{3,4}	0	0
	12	{3,9,5}	0	0
	13	{3,11,6}	0	1
14	{3,8,7}	0	0	

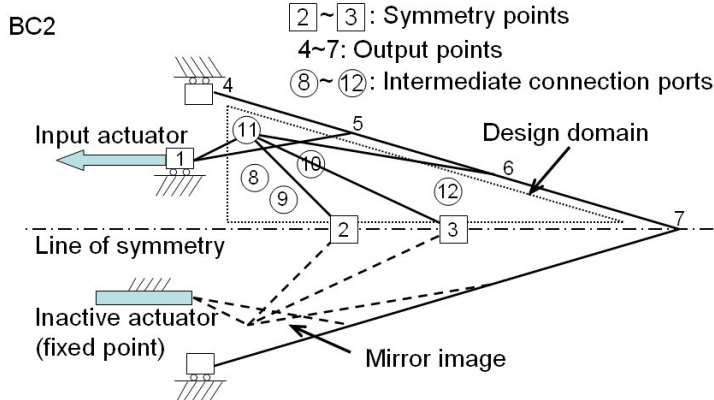


Figure 20: Effect of wandering connection port

The load-path representation was originally developed to synthesize shape morphing compliant mechanisms [12]. The objective is to minimize the shape deviation between a desired target shape and the structural boundary profile after shape morphing.

For the fin rib design, the same objective function is used to determine the optimal rib topology that can achieve a specific stroke motion. An exact target rib shape is not yet known or employed, but should propulsion be discovered to have a strong dependence on deformation shape, we will be able to generate custom mechanism designs to meet any arbitrary curve. In the meantime, the target rib profile is set to define a generic stroke deformation in one direction, based on the 10mm by 100mm initial rib design domain.

### A1.3. Genetic Algorithm

A genetic algorithm is then used to search for the optimal path connectivity (topology) allowing the rib to achieve the desired shape morphing with minimal least square error (LSE) shown in Eq. (7). The design variables include the path connectivity (pathSeq), the existence of each path (pTop<sub>i</sub>), the connection port locations (portX, portY), the in-plane path dimensions (pDim<sub>i</sub>), and the rib boundary dimension (h<sub>boundary</sub>). The variable bounds and the constraints are listed in Eq. (8)~(14). In the genetic algorithm, all the design variables are randomly generated in the first generation, and the optimal design can be obtained by evolving the initial population through many generations.

minimize *Least Square Errors (LSE)*

$$= \frac{1}{n} \sum_{i=1}^n \sqrt{(x_{DEF,i} - x_{TAR,i})^2 + (y_{DEF,i} - y_{TAR,i})^2} \quad (7)$$

Subject to

$$d = K^{-1}F \quad (8)$$

$$1mm \leq h_{Boundary} \leq 2mm \quad (9)$$

$$1mm \leq pDim_i \leq 2mm \quad (10)$$

$$h_e = pTop_i \times pDim_{i,j} \quad (11)$$

$$0.1mm \leq portX \leq 49.5mm \quad (12)$$

$$0.1mm \leq portY \leq 2.45mm \quad (13)$$

$$\sum_{i \in pathInOut} pTop_i \geq 1 \quad (14)$$

where pTop  $\in$  {0,1};

pDim, h<sub>boundary</sub>, portX, portY  $\in$   $\mathbb{R}^+$ ;

i: path number;

j: section number in the i<sup>th</sup> path;

e: element number.

### A1.4. Results

Figures 21 and 22 are the optimal topologies obtained from the genetic algorithm with BC1 and BC2, respectively. Although linear beam elements are used to solve for the large deformation seen in the rib structure, the linear analysis should be sufficient for determining the optimal topology. A non-linear analysis for large deformation is later incorporated in the size and geometry optimization stage for more accurate deformation and stress results.

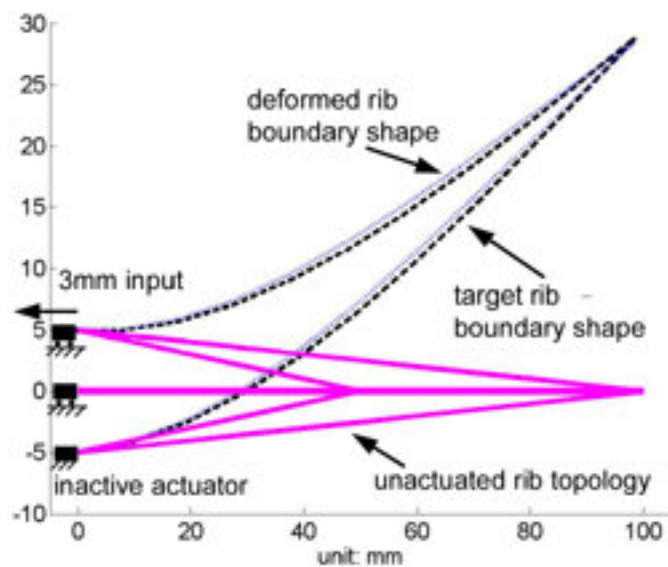


Figure 21: Design LP-BC1, generated by Load-Path Method

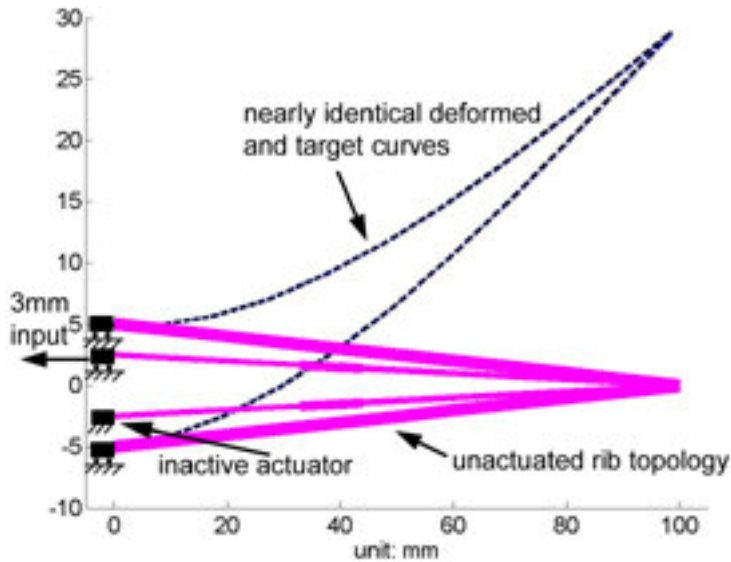


Figure 22: Design LP-BC2, generated by Load-Path approach

### A1.5. Discussion

The two topology synthesis approaches yielded different optimal topologies, partly because of the use of different objective functions, and partly because of the use of different optimization techniques. The continuous optimization method typically converges to a local optimum more efficiently, but the final solution is starting point dependent, and it also requires a filtering scheme to remove elements converging to the lower bound. The genetic algorithm is capable of searching the entire solution space more effectively, but the final solution is only 'close to' a local optimum. However, the binary variables used in the load-path representation allow clear representation of the structural connectivity, thus eliminating the need for a filtering scheme.

Of the designs for (BC1), the load-path topology is chosen because of its simplicity and additional compliance. The topology attained from the grounded-structure method is used for (BC2), because of the undesirable overlapping elements attained from the load-path method. Comments on the similarity of the load-path and grounded-structure methods will follow the results of size and geometry optimization (Section A3).

### A2. SIZE AND GEOMETRY OPTIMIZATION

The best designs of both topology generation methods were chosen for further refinement of size and geometry, i.e. the grounded-structure results for BC1 and the load-path results for BC2. Optimization was performed inside of a commercial FEA package (Ansys), using a first-order gradient method with line search. The parameters are different from those used in topology generation, because the topology is now fixed. Beam thickness is still a parameter, but cannot to go to zero (or a very small number). In addition, the locations of many of the nodes are allowed to wander within the design domain. In size and geometry optimization, maximum stress constraints are added to the formulation. Stress constraints are not possible in

topology generation, where beams with near-zero dimensions result in misleadingly high stresses.

$$\text{minimize } \frac{\text{Strain Energy}}{\text{Geometric Advantage}} \quad (15)$$

Subject to

$$d = K^{-1}F \quad (16)$$

$$0.5\text{mm} \leq h_{\text{boundary}} \leq 3\text{mm} \quad (17)$$

$$0.5\text{mm} \leq h_{\text{interior}} \leq 3\text{mm} \quad (18)$$

$$d_{\text{input}} \leq 5\text{mm} \quad (19)$$

$$d_{\text{tip}} \geq 15\text{mm} \quad (20)$$

$$\sigma_{\text{max}} \leq 34.45\text{MPa} \quad (21)$$

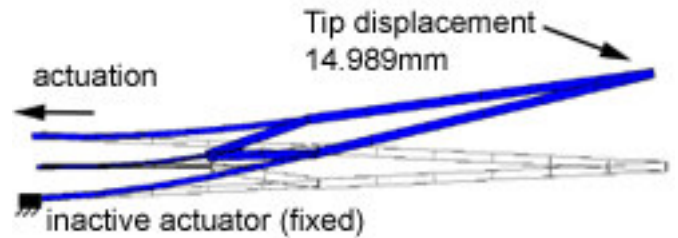


Figure 23: Design SS-BC1, based on GS-BC1

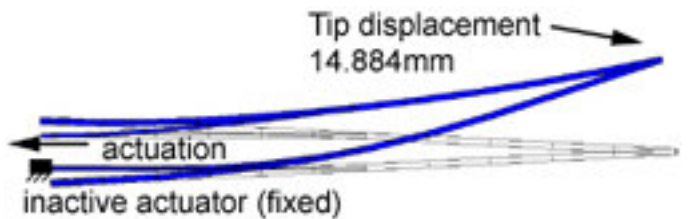


Figure 24: Design SS-BC2, based on LP-BC2

The topology depicted in Fig. 23 appears to be different from the topology used to form it, GS-BC1. This results from the two far-left interior nodes wandering to the same location. Because the two beams appear as one, they will be combined together in further analysis and fabrication.

### A3. DISCUSSION AND COMPARISON

While the original topologies attained from the synthesis methods in Sections A1.1 and A1.2 appear very different from each other, the subsequent size and geometry optimization illuminates similarities of results from both methods. Neither of the original topology optimization schemes guarantee a global solution, but the size and geometry optimization makes these comparisons possible. These similarities help to confirm the validity of using topology generation schemes to design compliant mechanisms.

Looking at the two final topologies for BC1 in Figs. 25 and 26, the comparison is evident. (Note that the overlapping elements from the load-path method have been eliminated to simplify the design.) The interior "Y" from the grounded-structure approach easily becomes the single beam of the load-path

approach, by sliding the connecting points to the tip. The diamond shaped structure at the end of the former design simply adds more stiffness to the tip of the rib.



**Figure 25:** Results for GS-BC1 after Size and Geometry Optimization



**Figure 26:** Design LP-BC1, simplified

Considering the resulting structures for BC2, topological similarities are again apparent. The structure attained from the grounded-structure method and a variation of its topology are shown in Figs. 27 and 28. The structural variation is very similar to the results attained from the load-path method shown in Fig. 29. The only difference is the beam that crosses the line of symmetry. As with BC1, this traverse beam stiffens the tip of the structure. Its deletion results in a more compliant structure, capable of more continuous curves.

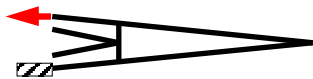


**Figure 27:** Design GS-BC2

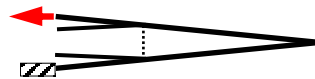


**Figure 28:** Topological Equivalent of Fig. 27



**Figure 29:** Design LP-BC2

## DIGITAL APPENDIX

The following videos can be found on our website:

[www.engin.umich.edu/~btrease/imece03](http://www.engin.umich.edu/~btrease/imece03)

- (1) pectoral-1.avi
- (2) pectoral-2.avi
- (3) undulating-fin.avi

## ACKNOWLEDGMENTS

The authors would like to thank Dr. B.R. Ratna and Dr. A. Srinivasan, of the Naval Research Laboratory for their collaboration on this project. K. Lu received financial support from the Naval Research Laboratory under Contract Number N66001-02-C-8061. B. Trease is supported by a National Science Foundation Graduate Research Fellowship. We acknowledge Zachary Kreiner, a Mechanical Engineering undergraduate student at the University of Michigan, for contribution of the Undulating Fin hydrofoil design.

## REFERENCES

- [1] Barthlott, W. and Neinhuis, C., 1997, "Purity of the sacred lotus or escape from contamination in biological surfaces," *Planta*, **202**, pp. 1-7.
- [2] Garner, L. J., Wilson, L. N., Lagoudas, D. C. and Rediniotis, O. K., 2000, "Development of a shape memory alloy actuated biomimetic vehicle," *Journal of Smart Materials and Structures*, **9**(5), pp. 673-683.
- [3] Rediniotis, O. K., Wilson, L. N., Lagoudas, D. C. and Khan, M. M., 2002, "Development of a Shape-Memory-Alloy

- Actuated Biomimetic Hydrofoil," *Journal of Intelligent Material Systems and Structures*, **13**(1), pp. 35-49.
- [4] Guo, S., Fukuda, T. and Asaka, K., 2003, "A new type of fish-like underwater microrobot," *IEEE/ASME Transactions on Mechatronics*, **8**(1), pp. 136-141.
- [5] Barrett, D. S., Triantafyllou, M. S., Yue, D. K. P., Grosenbaugh, M. A. and Wolfgang, M. J., 1999, "Drag Reduction in Fish-Like Locomotion," *Journal of Fluid Mechanics*, **392**, pp. 183-212.
- [6] Kumph, J. and Triantafyllou, M. S., 1998, "A fast-starting and maneuvering vehicle, the Robopike," *International Symposium of Seawater Drag Reduction*, Newport, RI, pp. 485-490.
- [7] Ananthasuresh, G. K., 1994, *A New Design Paradigm for Micro-Electro-Mechanical Systems and Investigations on the Compliant Mechanism Synthesis*, Department of Mechanical Engineering, University of Michigan, Ann Arbor.
- [8] Frecker, M., 1997, *Optimal Design of Compliant Mechanisms*, Department of Mechanical Engineering, University of Michigan, Ann Arbor.
- [9] Hetrick, J. A., 1999, *An Energy Efficiency Approach for Unified Topological and Dimensional Synthesis of Compliant Mechanisms*, Department of Mechanical Engineering, University of Michigan, Ann Arbor.
- [10] Joo, J., 2001, *Nonlinear Synthesis of Compliant Mechanisms: Topology and Size and Shape Design*, Mechanical Engineering, University of Michigan, Ann Arbor.
- [11] Lu, K. J. and Kota, S., 2003, "Design of Compliant Mechanisms for Morphing Structural Shapes," *Journal of Intelligent Material Systems and Structures* (in press).
- [12] Lu, K. J. and Kota, S., 2003, "Parameterization Strategy for Optimization of Shape Morphing Compliant Mechanisms Using Load Path Representation," *ASME 2003 Design Engineering Technical Conferences*, Chicago, IL, DETC2003/ DAC-48775.
- [13] Ramamurti, R., Sandberg, W. C., Lohner, R., Walker, J. A. and Westneat, M. W., 2002, "Fluid dynamics of flapping aquatic flight in the bird wrasse: three-dimensional unsteady computations with fin deformation," *Journal of Experimental Biology*, **205**, pp. 2997-3008.
- [14] Thomsen III, D. L., Keller, P., Naciri, J., Pink, R., Jeon, H., Shenoy, D. and Ratna, B. R., 2001, "Liquid Crystal Elastomers with Mechanical Properties of a Muscle," *Macromolecules*, **34**(17), pp. 5868-5875.